Adaptive mesh refinement for thermal-reactive flow and transport on unstructured grids

Jones, E.; De Hoop, S.; Voskov, D.

DOI
10.3997/2214-4609.202035218

Publication date
2020

Document Version
Final published version

Published in
ECMOR 2020 - 17th European Conference on the Mathematics of Oil Recovery

Adaptive Mesh Refinement for Thermal-Reactive Flow and Transport on Unstructured Grids

E. Jones[1*], S. De Hoop[1], D. Voskov[1,2]

[1] Delft University of Technology; [2] Stanford University

Summary

A coupled description of flow and thermal-reactive transport is spanning a wide range of scales in space and time, which often introduces a significant complexity for the modelling of such processes. Subsurface reservoir heterogeneity with complex multi-scale features increases the modelling complexity even further. Traditional Algebraic Multiscale techniques are usually focused on the accuracy of the pressure solution and often ignore the transport. Improving the transport solution can however be quite significant for the performance of the simulation, especially in complex applications related to thermal-compositional flow. The use of an Adaptive Mesh Refinement enables the grid to adapt dynamically during the simulation, which facilitates the efficient use of computational resources. This is especially important in applications with reactive flow and transport where the region requires high-resolution calculations as often localized in space. In this work, the aim is to develop an Adaptive Mesh Refinement framework for general-purpose reservoir simulation. The approach uses a multi-level connection list and can be applied to fully unstructured grids. The adaptivity of the grid in the developed framework is based on a hierarchical approach. First, the fine-scale model is constructed, which accurately approximates all reservoir heterogeneity. Next, a global flow-based upscaling is applied, where an unstructured partitioning of the original grid is created. Once the full hierarchy of levels is constructed, the simulation is started at the coarsest grid. Grid space refinement criteria can be developed specifically for a particular application of interest. The multi-level connectivity lists are redefined at each timestep and used as an input for the next. The developed Adaptive Mesh Refinement framework was implemented in Delft Advanced Research Terra Simulator which uses the Operator-Based Linearization technique. The performance of the proposed approach is illustrated for several applications, including hydrocarbon production, geothermal energy extraction and subsurface storage.

Introduction

Production development of prospective reservoirs includes the use of various technologies that provide information at many different scales. These scales range from core plugs being a few centimeters in size to well logs detecting properties a few meters around the well, and to seismic imaging covering a significant volume with limited resolution (few meters vertically and 10's of meters horizontally). However, time and capital limitations result in sparse direct sampling of reservoir rock and fluid properties. This is why the construction of reservoir models, through integration of these data using geostatistical reservoir description algorithms, has become a crucial step in resource development (Branets et al., 2009). These algorithms conventionally result in fine-scale descriptions of reservoir properties (porosity, permeability) on grids of tens of millions of cells (Christie, 1996).

An issue of considerable importance is the risk and uncertainty assessment of reservoir performance. The uncertainty can be gauged by simulating an ensemble of different geological realizations. This may require to run thousands of simulations to cover a wide range of parameter variation. It is however not computationally feasible or desirable to perform these simulations on the high-fidelity (fine-grid) model. Significantly upscaled models (i.e., the mapping of rock and fluid properties to a coarser resolution) are therefore required, where these models should ideally be even coarser than typical reservoir simulators, which can handle on the order of $10^5 - 10^6$ simulation cells (Durlofsky, 2005). In the presence of more complex physics, excessive upscaling may, however, result in non-satisfactory results, which necessitate the use of advanced algorithms and solvers to allow for higher resolution grids to be employed (Cusini et al., 2016).

Traditional Algebraic Multiscale techniques (Jenny et al., 2003; Wang et al., 2014), developed to solve the elliptic (or parabolic) pressure equation in sequentially coupled simulations, mainly focus on the pressure solution and often ignore the transport. However, in complex applications related to chemical and compositional EOR (Enhanced Oil Recovery), reservoir storage and geothermal industry, the number of conserved chemical species can be large which makes any improvement in transport solution quite significant for the performance and robustness of the simulation. A technique called *Adaptive Mesh Refinement* (AMR) provides an effective means for adapting the resolution of a model to solution requirements. This method is well developed in many areas of computational physics (e.g. fluid dynamics and solid mechanics) but is however not widely used for practical reservoir simulation (Karimi-Fard & Durlofsky, 2014).

In today's literature, several researchers have developed and proposed AMR procedures to capture the local nature of transport processes. Bahrainian and Dezfuli (2014) have developed a novel unstructured grid generation algorithm which considers the effect of geological features and well locations in the grid resolution. This strategy involves the definition and construction of the initial grid based on the geological model, geometry adaptation of geological features and grid resolution control. Trangenstein (2002) used the combination of high-resolution discretization methods with dynamically adaptive mesh refinement for a two-component single-phase model for miscible flooding. Pau et al. (2012) proposed an AMR algorithm for compressible two-phase flow in porous media. The method is implemented within a block structured adaptive mesh refinement framework which allows the grids to dynamically adapt to flow features and enables efficient parallelization of the algorithm. The coarse-scale permeability was obtained by averaging the fine-scale permeability. Similar techniques have been developed for compositional simulation (Sammon et al., 2003), thermal problems (Christensen et al., 2004), improved/enhanced oil recovery processes (Van Batenburg et al., 2011) and many more applications.

In this work, the aim was to develop a dynamic AMR scheme using an unstructured multi-level gridding framework, for general-purpose reservoir simulation. The focus lied particularly on thermal-reactive flow and transport formulation which are required for a wide range of subsurface applications. First, a fine-scale geological model was constructed accurately, approximating all reservoir heterogeneity. This model is represented by a list of volumes, depths and a connectivity list (Lim et al., 1995) describing each control volume. Next, a global flow-based upscaling was applied and an unstructured partitioning of the original grid was constructed as suggested in (Karimi-Fard & Durlofsky, 2014). This partitioning

provides coarser levels of the original model each of which is also described by a list of volumes, depths and a connectivity list. A coarser connectivity list includes connections between control volumes at the given level as well as interconnections between the levels. Once the full hierarchy of levels is constructed, the simulation is started at the coarsest grid. Grid space refinement criterion is developed for particular applications. The multi-level connection list is reconstructed at each time step and used for the simulation. The proposed approach was implemented in *Delft Advanced Research Terra Simulator* (DARTS) which is based on Operator-Based Linearization techniques (Voskov, 2017).

Methodology

Governing equations

General-purpose reservoir simulation is based on the solution of governing equations which describe mass and energy transfer of various species in the subsurface. The flow of mass and energy in a system with n_p phases and n_c components are described in this section. For this general-purpose thermal-compositional model, n_c component mass conservation equations and a single energy conservation equation need to be solved (Khait & Voskov, 2018b). When chemical reactions occur in the system, an additional term describing n_k kinetic reactions is added on the right-hand side of the mass conservation equation. These governing relations are described as:

$$\frac{\partial}{\partial t}\left(\phi \sum_{p=1}^{n_p} x_{cp}\rho_p s_p\right) + \mathrm{div}\sum_{p=1}^{n_p} x_{cp}\rho_p u_p + \sum_{p=1}^{n_p} x_{cp}\rho_p \tilde{q}_p = \sum_{k}^{n_k} v_{ck} r_k, \quad c = 1,\ldots,n_c, \quad k = 1,\ldots,n_k, \quad (1)$$

$$\frac{\partial}{\partial t}\left(\phi \sum_{p=1}^{n_p} \rho_p s_p U_p + (1-\phi)U_r\right) + \mathrm{div}\sum_{p=1}^{n_p} h_p \rho_p \overrightarrow{u_p} + \mathrm{div}(\kappa \nabla T) + \sum_{p=1}^{n_p} h_p \rho_p \tilde{q}_p = 0, \quad (2)$$

where t is the time, v_{ck} is the stoichiometric coefficient associated with kinetic reaction k, r_k is the rate of kinetic reaction k. The right-hand side of the mass conservation equation 1 is the kinetic term which describes reactions. It is set to zero when no chemical processes are involved in the system. The rest of the terms in the system can be described as functions of spatial coordinate ξ and/or physical state ω:

$\phi(\xi,\omega)$: porosity,
$x_{cp}(\omega)$: the mole fraction of component c in phase p,
$s_p(\omega)$: phase saturation,
$\rho_p(\omega)$: phase molar density,
$\overrightarrow{u_p}(\xi,\omega)$: phase velocity,
$\tilde{q}_p(\xi,\omega,\mathbf{u})$: source of phase p,
$\mathrm{U}_p(\xi)$: phase internal energy,
$\mathrm{U}_r(\xi)$: rock internal energy,
$h_p(\xi)$: phase enthalpy,
$\kappa(\xi,\omega)$: thermal conduction.

An exception is the phase source term, which is also dependent on $\mathbf{u}$ - well control variables.

The rock internal energy and thermal conduction are assumed to be spatially homogeneous for simplification of the problem, meaning that they are characterized as functions of the spatial coordinate ω only. Phase flow velocity $\overrightarrow{u_p}$ is assumed to follow Darcy's law, expressed as:

$$\overrightarrow{u_p} = -\left(\mathbf{K}\frac{k_{rp}}{\mu_p}\left(\nabla P_p - \overrightarrow{\gamma}_p \nabla D\right)\right), \quad p = 1,\ldots,n_p, \quad (3)$$

where

$\mathbf{K}(\xi)$: permeability tensor,
$k_{rp}(\omega)$: relative permeability of phase p,
$\mu_p(\omega)$: phase viscosity,
$P_p(\omega)$: pressure in phase p,
$\overrightarrow{\gamma}_p(\omega)$: gravity vector,
$D(\xi)$: depth (backward oriented).

The nonlinear unknowns in this system of equations are the pressure P, the overall compositions z_c of each component and the enthalpy h.

Modeling approach

In order to solve the governing equations 1 and 2, we apply a finite-volume discretization on a general unstructured mesh and perform a backward Euler approximation in time to both equations, where the phase velocities $\overrightarrow{u_p}$ are substituted by the Darcy relation (3):

$$V\left[\left(\phi\sum_{p=1}^{n_p}x_{cp}\rho_p s_p\right)^{n+1}-\left(\phi\sum_{p=1}^{n_p}x_{cp}\rho_p s_p\right)^{n}\right]-\Delta t\sum_l\left(\sum_{p=1}^{n_p}x^l_{cp}\rho^l_p\Gamma^l_p\Delta\psi^l\right), \\ +\Delta t\sum_{p=1}^{n_p}\rho_p x_{cp}q_p=V\Delta t\sum_k^{n_r}v_{ck}r_k,\quad c=1,\ldots,n_c \tag{4}$$

$$V\left[\left(\phi\sum_{p=1}^{n_p}\rho_p s_p U_p+(1-\phi)U_r\right)^{n+1}-\left(\phi\sum_{p=1}^{n_p}\rho_p s_p U_p+(1-\phi)U_r\right)^{n}\right] \\ -\Delta t\sum_l\left(\sum_{p=1}^{n_p}h^l_p\rho^l_p\Gamma^l_p\Delta\psi^l+\Gamma^l_c\Delta T^l\right)+\Delta t\sum_{p=1}^{n_p}h_p\rho_p q_p=0. \tag{5}$$

Here V is the control volume for which the system is being solved, $q_p=\tilde{q}_pV$ is a source of phase p, n is the previous time step whereas $n+1$ is the time step we want to solve for. Capillarity and gravity are neglected in these equations, and a Two-Point Flux Approximation (TPFA) with an upstream weighting is applied. $\Delta\psi^l$, the phase potential, therefore simply becomes the difference in pressure between blocks connected via interface l, while ΔT^l is the temperature difference between these blocks; $\Gamma^l_p=\Gamma^l k^l_{rp}/\mu^l_p$ is a phase transmissibility, where Γ^l is the constant geometrical part of the transmissibility (involving permeability and geometry of the control volume). Finally $\Gamma^l_c=\Gamma^l\kappa$ is the thermal (conductive) transmissibility (Khait & Voskov, 2018b). This system of equations is solved for each mesh element in time, where the unknowns are the composition of the n_c components and the pressure for the mass conservation equation (4), and the pressure and enthalpy for the energy equation (5).

In general-purpose reservoir simulation, the solving process requires the linearization of strongly nonlinear governing equations. In conventional reservoir simulators, a Newton-Raphson based method is typically used for the linearization, which solves on each nonlinear iteration a linear system of equations in the following form:

$$J(\omega^n)(\omega^{n+1}-\omega^n)=-r(\omega^n), \tag{6}$$

where r is the residual and J is the Jacobian, which is the derivative of the residual with respect to primary nonlinear unknowns, defined at a nonlinear iteration n. In this work, we use a recently-developed approach called *Operator Based Linearization* (OBL). The main idea of OBL is to transform the discretized mass and energy conservation equations (4 and 5) to an operator form, where space-dependent ξ and state-dependent ω properties of governing equations are separated. This provides the opportunity to approximate the representation of the exact physics of a problem through the discretization of the state-dependent properties. The underlying methodology of OBL is explained in more detail in Voskov (2017) and Khait and Voskov (2017, 2018a, 2018b).

Connectivity list

The proposed AMR technique uses the Finite Volume Method (FVM) for discretization. The implementation of the finite volume discretization method to the mass conservation equation 1 requires the evaluation of the flow between two adjacent control volumes in terms of the cell pressures. Using a Two-Point Flux Approximation (TPFA), the flow rate is defined as:

$$Q_{ij} = \Gamma_p^{ij}(P_i - P_j), \tag{7}$$

where:

Q_{ij} : flow rate at interface of cells i and j,
Γ_p^{ij} : phase transmissibility at interface of cells i and j,
P_i : pressure of cell i,
P_j : pressure of cell j.

Similarly, the heat flux between two adjacent control volumes is expressed in terms of thermal transmissibility Γ_c and is, also using a TPFA, defined as:

$$Q_{ij}^h = \Gamma_c^{ij}(T_i - T_j), \tag{8}$$

where Γ_c^{ij} is the thermal transmissibility at interface ij, T_i and T_j are the temperatures of cell i and j respectively, and Q_{ij}^h is the heat flux at interface ij.

To evaluate the flux between two adjacent control volumes, a so-called *connectivity list* is constructed, i.e. for each interface between two neighbouring control volumes, the indices of these cells are listed together with the transmissibility (Lim et al., 1995). The result is a list with all connection pairs present in the grid. A few important points to be noted are:

- Each connection consists of only two elements,
- The connection pairs are not repetitive,
- No-flow boundaries imply the absence of connections and are hence not listed in the connectivity list.

The figure below shows a simple example of a 2D Cartesian structured grid, with corresponding cell indexing. Table 1 shows its connectivity list. The list is expressed as two arrays, cell i and cell j, where each column represent a connection pair. Each pair has an associated interface transmissibility stored in the connectivity list.

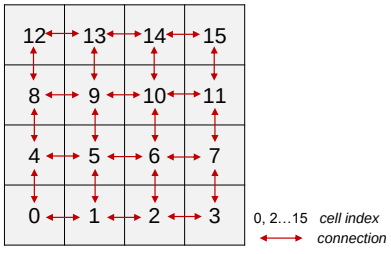

Figure 1 *4x4 Cartesian grid denoting cell indexing and showing neighbouring connections. Indexing is based on a Cartesian structured mesh for simplicity.*

Multi-level grid generation

The adaptivity of the grid in the developed AMR scheme is based on a hierarchical representation of connectivity list. The simulation grid is composed of several predefined *levels* representing the same

Table 1 *Connectivity list of the example grid from figure 1.*

	Dual connections																							
Cell *i*	0	0	1	1	2	2	3	4	4	5	5	6	6	7	8	8	9	9	10	10	11	12	13	14
Cell *j*	1	4	2	5	3	6	7	5	8	6	9	7	10	11	9	12	10	13	11	14	15	13	14	15

geological properties at different resolutions. We start with a fine-scale model (*static geological model*) which accurately represents all reservoir heterogeneity. This grid is defined as *level 0* and represents our finest level. The modeling grid is defined by a list of control volumes, depths, reservoir properties (all spatially distributed properties required to solve the discretized relations 4 and 5) for each mesh element, and a list of connectivity with corresponding transmissibility between neighbouring cells.

Next, *level 1* is defined, where control volumes are constructed by aggregating fine grid cells. Upscaling is applied to redefine volume, depth and reservoir properties at a coarser level. A connectivity list, with corresponding transmissibility, is constructed for this level and inter-level connections are defined in addition. Similarly, more levels of coarsening can be constructed. A control volume in grid-level n always consists of cells from grid-level $(n-1)$, resulting in a hierarchical relationship (Karimi-Fard & Durlofsky, 2014). The simulation grid is then obtained by combining control volumes from grids of different levels. A schematic representation of this procedure is illustrated in figure 2 below.

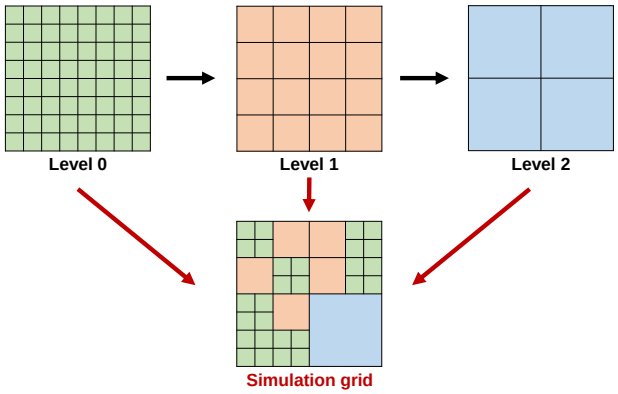

Figure 2 *2D Multi-level grid with three pre-constructed grids (levels) with an example simulation grid which is constructed by aggregating control volumes from different levels.*

Cell aggregation

A mesh consists of a set of finite elements, each having vertices with allocated coordinates. To conduct cell aggregation, the centroid is first computed for each mesh element within the grid. Figure 3 shows an example 2D unstructured grid to illustrate how cell aggregation is conducted. As can be seen, in this particular example, each cell has 3 vertices, and a centroid (represented in red) with coordinates x_c and y_c defined as $\left(\frac{x_1+x_2+x_3}{3}, \frac{y_1+y_2+y_3}{3}\right)$, where x_i and y_i are the coordinates of the vertices. Each mesh element has an assigned index number.

Cell aggregation is then carried out by dividing the grid in the x- and y-direction (and in the z-direction for 3D models) into equidistant intervals Δx and Δy using a predefined scaling factor. Figure 3 shows the range partitioning (illustrated by the white lines) for a 2D unstructured grid. The x- and y-range were divided in 5 and 3 equidistant intervals respectively. The yellow-highlighted 2D plane has range $[i, i+\Delta x]$ in the x-direction and $[j, j+\Delta y]$ in the y- direction. For this given example, all cell centroids whose coordinates fall within this plane, are aggregated to form one coarse cell. I.e., cells 41, 46, 68, 77, 84, 92, 106, 111 and 118 form coarse cell 0.

For the given 2D unstructured grid example in figure 3, the so-called *level 1* - i.e. the next level of coarsening - is shown in figure 4. The numbers represent the assigned indices of the newly constructed

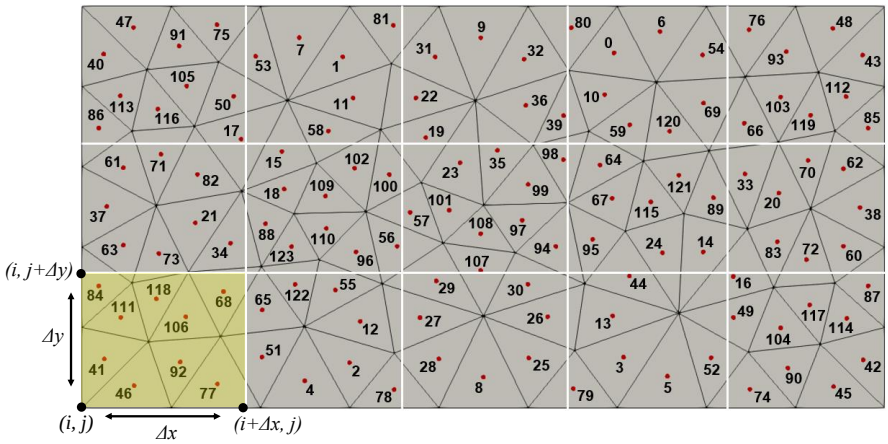

Figure 3 *2D unstructured grid with centroids and with range partitioning (represented by the white lines) in the x- and y-direction with Δx and Δy spacing respectively. Aggregation is carried out for cells whose centroid fall within a given x- ($[i : i+\Delta x]$) and y-range ($[j : j+\Delta y]$). E.g., all cells whose centroids are found within the yellow-highlighted 2D range are aggregated to form one coarse cell.*

coarse cells. If one wants to construct an additional level, the same procedure can be followed with a larger *x*- and *y*-range partitioning, where grid cells of level 1 are aggregated to form level 2.

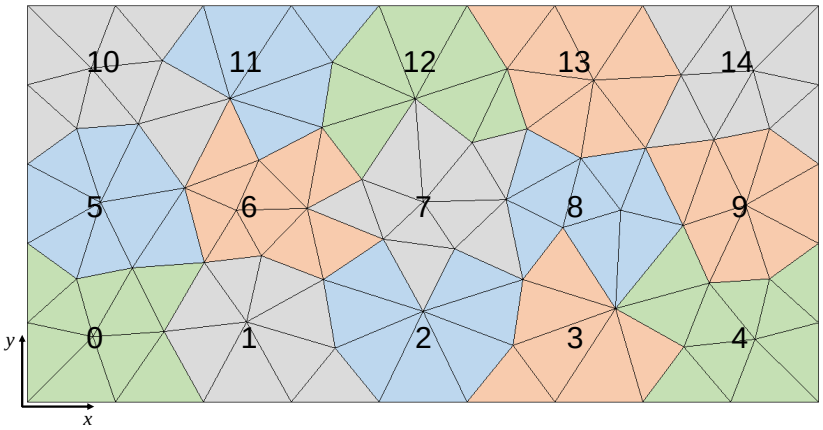

Figure 4 *2D unstructured grid of figure 3 after cell aggregation. This grid represents the next level of coarsening of the finest grid: level 1.*

For further steps into the construction of the levels, a list - *"fines in coarse"* - is constructed where the corresponding indices of the aggregated fine cells are listed for each coarse cell. Note that cell aggregation can also be conducted while taking care of highlighting geological features (e.g. fractures) and different facies in the model. For example, cell aggregation can be conducted by grouping domains with the same facies together into one coarse cell, or, in fractured reservoirs, by aggregating cells by isobar contours similar to (Karimi-Fard & Durlofsky, 2014). After cell aggregation is conducted, the connectivity list is then constructed describing all connections within each level and the inter-level connections.

Transmissibility and upscaling

In this work, the AMR method is implemented for unstructured grids of any geometry. The definition of the transmissibility for unstructured grids is expressed as:

$$\Gamma_p^{12} = \Gamma^{12}\lambda \quad \text{with} \quad \Gamma^{12} = \left(\frac{\alpha_1\alpha_2}{\alpha_1+\alpha_2}\right) \quad \text{and} \quad \alpha_i = A\frac{k_i}{D_i}n\cdot d_i, \tag{9}$$

where:

Γ_p^{12} : transmissibility between cells 1 and 2,
Γ^{12} : constant geometrical part of the transmissibility,
λ : mobility of a given phase p,
A : interface area,
k_i : permeability of cell i,
D_i : distance between centroid of cell i to interface area A,
n : unit vector normal to the interface,
d_i : unit vector along the line joining centroid of cell i to the center of interface A.

Here, the directional permeability of each cell is expressed as the magnitude of the cell's $[k_x, k_y, k_x]$ coordinates multiplied by the unit vector d_i.

To solve the mass conservation equation (eq. 1), the flow rate must be computed for the interface of every neighbouring cells. It is therefore necessary to compute the transmissibility for each dual connection listed in the connectivity list. The result is a list consisting of all connections, with their corresponding transmissibility. This methodology is applied at the finest level of refinement, level 0.

For thermal problems, another type of transmissibility Γ_c^l must be computed to approximate thermal conductive flux in the energy equation 2. Since thermal rock conduction is not as heterogeneous as permeability, the thermal transmissibility is defined as the geometric coefficient, that is, the area of the interface l divided by the sum of the distances D_1 and D_2 from centroids to interface l, multiplied by the average conduction κ_{12}:

$$\Gamma_c^{12} = \kappa_{12} \frac{A}{D_1 + D_2}. \tag{10}$$

As mentioned earlier, level 0 is represented by a list of volumes, depths and reservoir properties which are derived from the static geological model. Once the hierarchical grid is constructed, all cell properties must be redefined for the coarser levels (level > 0). This is done by upscaling the properties of the corresponding fine grid cells. The volume is upscaled by simply summing the volumes of the aggregated fine grid cells v_i;

$$V_I = \sum_{i \in I} v_i. \tag{11}$$

Depth upscaling is done by taking the average of the fine scale depths. The porosity, thermal conductivity, and rock heat capacity are upscaled using a volumetric averaging. For example, the sum of the porosity ϕ_i multiplied by the corresponding cell volume v_i of each fine cell i is taken over the total volume of the coarse cell V_I;

$$\bar{\phi}_I = \frac{1}{V_I} \sum_{i \in I} v_i \phi_i. \tag{12}$$

In this study, for the upscaling of permeability, we use the flow-based upscaling technique developed by (Karimi-Fard et al., 2006; Gong et al., 2008; Karimi-Fard & Durlofsky, 2012). This technique uses the pressure solution when the system has reached steady-state to compute the flow across each interface. The transmissibility can then be derived by rearranging the flow equation 7. These approaches can be applied to unstructured coarse grids with generally-shaped control volumes (Karimi-Fard & Durlofsky, 2014). The coarsening technique defines the coarse transmissibility Γ_p^{IJ} between two adjacent control volumes I and J. This is expressed as:

$$\Gamma_p^{IJ} = \left| \frac{Q_{IJ}}{P_I - P_J} \right|. \tag{13}$$

The coarse-grid average pressures P_I and P_J, and the coarse-grid flow rate Q_{IJ}, are computed using a fine-grid pressure solution. These quantities are given by:

$$P_I = \frac{1}{V_I} \sum_{i \in I} v_i p_i, \quad P_J = \frac{1}{V_J} \sum_{j \in J} v_j p_j, \quad Q_{IJ} = \sum_{(i \in I, j \in J)} Q_{ij} = \sum_{(i \in I, j \in J)} \Gamma_p^{ij} (p_i - p_j), \tag{14}$$

where p_i and p_j define the fine-scale pressures in the corresponding coarse blocks. In the flow rate expression Q_{ij}, ij indicates the interface between fine cells i and j and Γ_p^{ij} denotes the transmissibility for this interface. This ij interface comprises a portion of the interface between coarse blocks I and J. For inter-level connections, a similar approach is used. For a given fine cell i and coarse cell J with interface iJ, equation 14 is used with $P_I = p_i$, the pressure of fine cell i, and P_J the pressure of coarse cell J. This procedure is conducted for each inter-level connection found within the hierarchical grid.

For thermal problems, a similar method can be implemented, but is however not computationally efficient as temperature takes significantly longer to reach a steady state. We therefore use equation 10 to compute the upscaled thermal transmissibility, where the area is expressed as the sum of the fine-scale faces which compose interface IJ, and the distances D_I and D_J represent the distances between the cell centroid and the centroid of the coarse interface.

Dynamic adaptivity framework

To determine whether grid adaptivity is necessary, we define refinement and coarsening criteria, which are dependent on the application used. In this study, we adopted an approach where the difference in solution variable is analysed between neighbouring blocks. Therefore, the difference in the solution variable of interest X is computed between each pair of cells active in the simulation grid. If this difference is higher than a given threshold, both neighbouring blocks are refined. For the coarsening of a set of fine cells, belonging to a given coarse cell, the difference between all the corresponding fine cells and their neighbouring cells is computed; if each and every one of these connections have a difference in solution variable below a given threshold, the fine cells are coarsened to the next consecutive level.

For cells marked for refinement, the corresponding fine cells from the level below are added to the list of active blocks, which is used for implementation of the next time step, while the indices of the coarse cells in question are suppressed. Similarly, the cells marked for coarsening are suppressed from the active cells, and the corresponding coarse blocks are added. Figure 5 below shows an example of a two-level hierarchical grid. The current time step simulation grid is represented on the bottom left. After a check for adaptivity was conducted, cells 1 and 2 were marked for refinement. Hence as explained above, the cell indices 1 and 2 are suppressed from the list of active blocks, and their corresponding fine cell indices are added (6, 7, 10 and 11 for coarse cell 1, and 12, 13, 16 and 17 for coarse cell 2). The scheme at the bottom right of the figure shows the simulation grid which will be used for the next time step. Cell adaptivity results in an unstructured indexing as shown in the figure below.

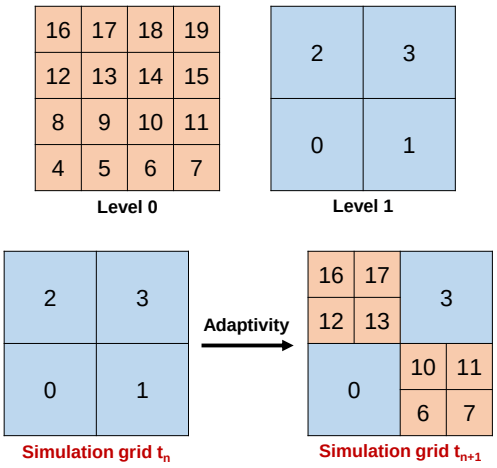

Figure 5 *Schematic representation of a 2-level hierarchical grid, with illustrated the adaptivity procedure and the redefinition of the active blocks for the simulation grid of the next time step t_{n+1}.*

Once the simulation grid is redefined and the list of active cells is updated, the connectivity list and corresponding transmissibility must be redefined. This is done by copying the list of connections for the

whole hierarchical grid, where only the connections and corresponding transmissibility involving the active cells are kept, while connections involving non-active cells and their corresponding transmissibility are suppressed. Similarly, the same holds for the list of volume, depth and relevant properties. Only the cell properties of the active blocks are stored.

For computation of the next time step solution X_{n+1}, the solution of the previous time step X_n is required (see equations 4 and 5). However, X_n doesn't have the same grid configuration as the next time step t_{n+1}. It is therefore necessary to convert the grid of solution X_n to the same configuration as the simulation grid at t_{n+1}. To do so, we use simple mapping techniques. A prolongation operator is firstly used to redefine the solution variable X at each cell of the finest level of refinement (level 0). A so-called *constant prolongation* is implemented; i.e., all sub-domain values X_i are set to the coarse value solution variable X_I:

$$X_i = X_I, \quad \forall i \in I. \tag{15}$$

Subsequently, restriction to the new simulation grid is conducted on the prolongated solution; i.e., for cells already at the finest level, the solution stays the same; when several control volumes are grouped into a single coarser control volume, the coarse value X_I is set to the volume-weighted average of all sub-domain values X_i (Karimi-Fard & Durlofsky, 2014):

$$X_I = \frac{1}{V_I} \sum_{i \in I} v_i X_i. \tag{16}$$

A schematic representation of this procedure for the 2-level hierarchical grid and for the new simulation grid of figure 5 (t_{n+1}) is shown in figure 6 below.

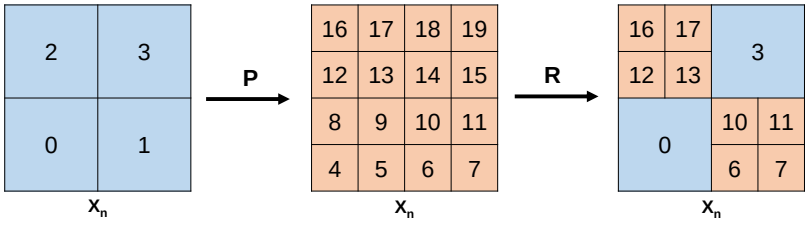

Figure 6 *Schematic representation of the prolongation and restriction for the example in figure 5.*

Applications for Geothermal Reservoirs

Geothermal technology has recently received substantial attention as an alternative source of energy. However, geothermal production systems have a relatively low return on investment, where uncertainties related to lack of detailed information about subsurface formations can significantly affect the quantification of the economic planning and feasibility of geothermal projects (Willems, 2017). It is therefore important to reduce the uncertainty and produce a high accuracy solution while keeping the computational costs low. Geothermal systems therefore represent a good candidate for implementation of our AMR framework since it keeps the accuracy of simulation process close to the fine-scale while the performance is close to coarse-scale models.

Simulation of geothermal reservoirs implicates the solution of both mass (1) and energy (2) conservation equations where pressure and enthalpy are the solution variables. We are mostly interested in the accurate prediction of the temperature displacement front and resulting thermal breakthrough time. Dynamic adaptivity will be illustrated for 2 synthetic geothermal examples:

- A homogeneous reservoir with unstructured meshing,
- A heterogeneous fluvial system from (Shetty et al., 2017) with low net-to-gross ratio.

In *DARTS*, the enthalpy is used as nonlinear unknown instead of the temperature. The adaptivity criteria are therefore applied to the enthalpy solution where the difference in enthalpy between two adjacent

control volumes is analysed. This is done for each pair of connection within the simulation grid. Here, we applied the following adaptivity criteria:

$$\begin{cases} \text{if } \Delta h_{ij} > 70\ kJ, & \text{mark cells i and j for refinement,} \\ \text{if } \Delta h_l < 40\ kJ, \quad \forall l \in I, & \text{mark cells } \{\forall i \in I\} \text{ for coarsening.} \end{cases} \tag{17}$$

The geothermal examples are illustrated by showing the fine-scale solution at different time steps versus the AMR solution and the coarse-scale solution. Each synthetic example was analyzed quantitatively by conducting an error analysis where the error of both AMR and coarse solution are computed relative to the fine-scale solution. Both the L2 norm and L-infinity norm were calculated for each time step throughout the simulation. Moreover, to define the performance of the AMR method in terms of computational resources, the percentage of grid cells utilized in the simulation using the AMR grid, relative to the total number of cells in the fine-scale model was plotted for each example.

Homogeneous model

The first model is a simple 2D homogeneous reservoir (constant permeability) with unstructured triangular mesh. We consider a single injector (I) and a single producer (P) configuration. A two-level hierarchical grid is used, with 1420 cells in level 0 and 75 cells in level 1. Figure 7 below illustrates both levels, along with the permeability field (constant permeability of 2000 mD), and the well locations. The level 1 is illustrated above where each color represents a coarse cell. As can be seen, cell aggrega-

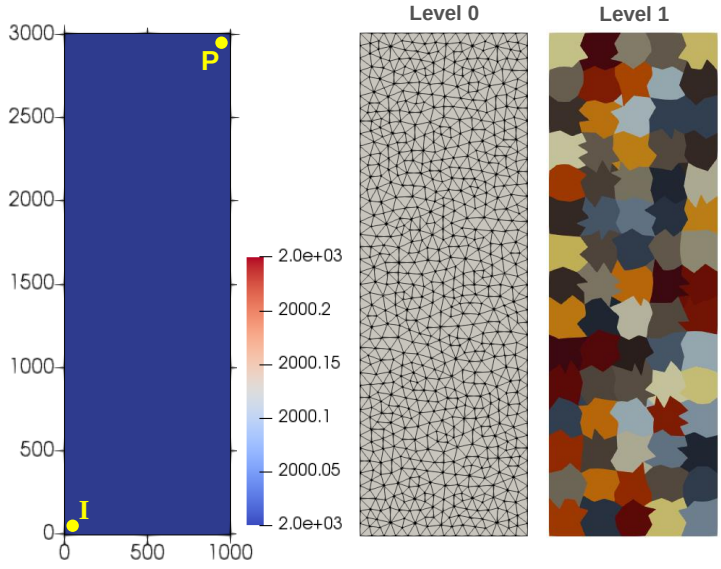

Figure 7 *Hierarchical grid of the unstructured homogeneous model. Left figure: permeability field with reservoir dimensions and well locations; middle figure: level 0, the finest level of refinement, with unstructured gridding; right figure: coarser level, level 1 where each color represents a coarse cell.*

tion was conducted by dividing the x- and y- axes into 5 and 15 equidistant intervals. The cells at the well locations are kept fine at all times. The simulation was conducted for a period of 5500 days. The temperature solution at three different times is shown in figure 8. Figure (a) represents the temperature solution at fine scale, figure (b) the solution on the AMR grid, figure (c) shows the coarse-scale solution, and figure (d) shows the node distribution for the AMR simulation run.

The solution on the AMR grid demonstrates a particularly good match with the fine-scale solution. The node distribution shows high concentration along the front and at the well locations, and low concentration behind and ahead of the front, where no significant changes are observed. This considerably lowers the computational time as compared to running the fine-scale model. The coarse-scale solution differs notably from the AMR and fine-scale solution, with a faster cold front propagation at the coarse grid which is more pronounced in comparison at late times $t_D = 0.3$ and 1.

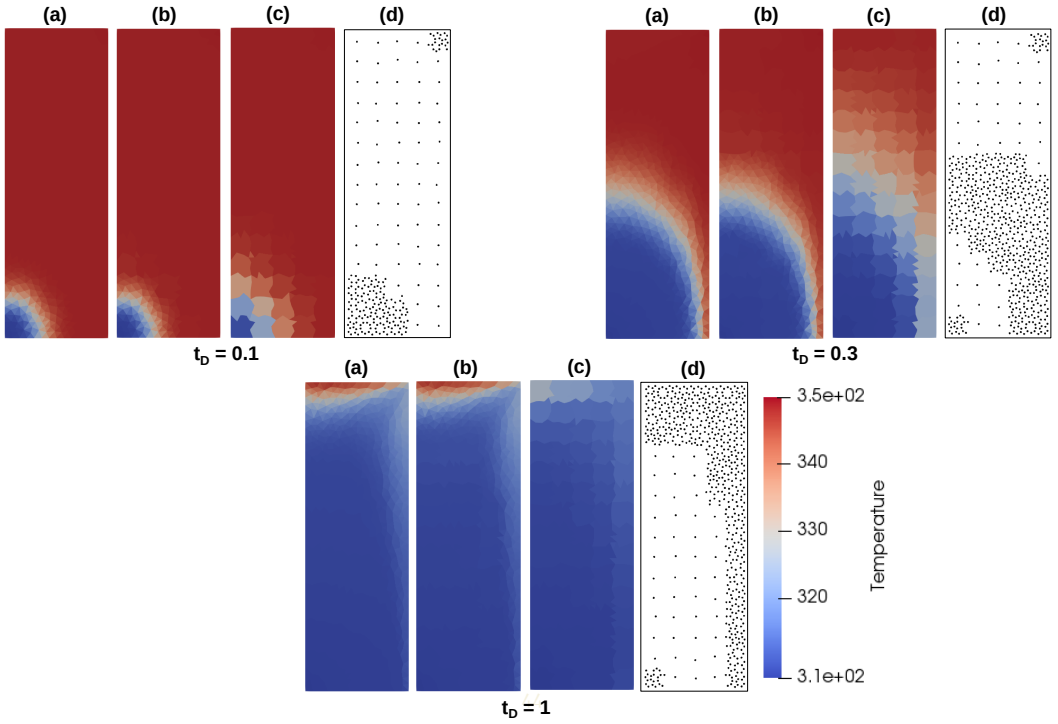

Figure 8 *Temperature solution of the homogeneous reservoir with unstructured gridding at t_D = 0.01, 0.3 and 1. (a) represents the fine-scale solution; (b) represents the AMR solution; (c) is the coarse-scale solution; (d) is the node distribution of the AMR grid.*

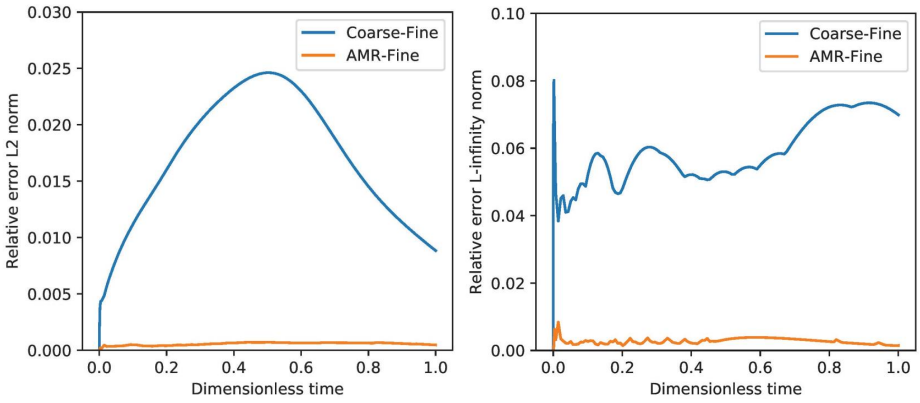

Figure 9 *L2 norm (left) and L-infinity norm (right) of the difference between the coarse model and the fine model, and between the AMR model and the fine model, both relative to the fine-scale solution, for the homogeneous model with unstructured gridding from figures 7 to 8.*

The relative error of the AMR solution is significantly lower than the coarse solution in both the L2 and L-infinity norm (figure 9). Moreover, the amount of cells is considerably reduced (see figure 10), ranging from 8 to 60%. The trend shows an overall increase as the front propagates, and a decrease when the cold front has reached the producing well, which results in coarsening at locations where no more thermal variations are detected. This considerably improves the performance of simulation since the AMR approach is much more favourable in terms of efficient use of computational resources.

Fluvial heterogeneous model

Our AMR framework was tested for a heterogeneous reservoir with a low net-to-gross ratio (N/G = 35%). The permeability field ranges from 5 to 3400 mD with a significant amount of shale regions present. The hierarchical grid for this example is a structured grid and it comprises two levels. The finest grid, level 0,

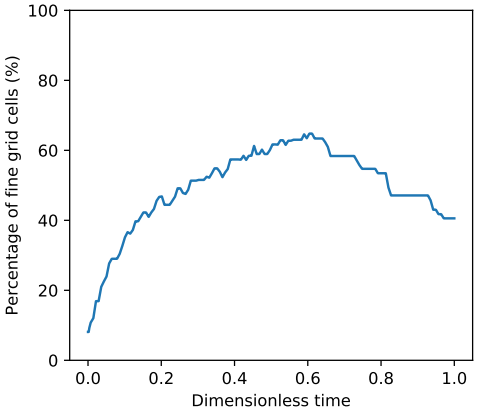

Figure 10 *Percentage of mesh elements used during the simulation of the AMR model, relative to the total number of cells in the fine-scale model in time for the homogeneous model from figures 7 to 8.*

consists of 2400 grid cells with 40 cells in the x-direction and 60 cells in the y-direction. Level 1 was reduced to 150 mesh elements, where aggregation was done using 4x4 fine mesh elements, resulting in 10 grid cells in the x-direction and 15 grid cells in the y-direction. The permeability field along with the hierarchical grid for this example is shown in figure 11 below. The location of the injector (I) and producer (P) are depicted in yellow on the permeability distribution figure below.

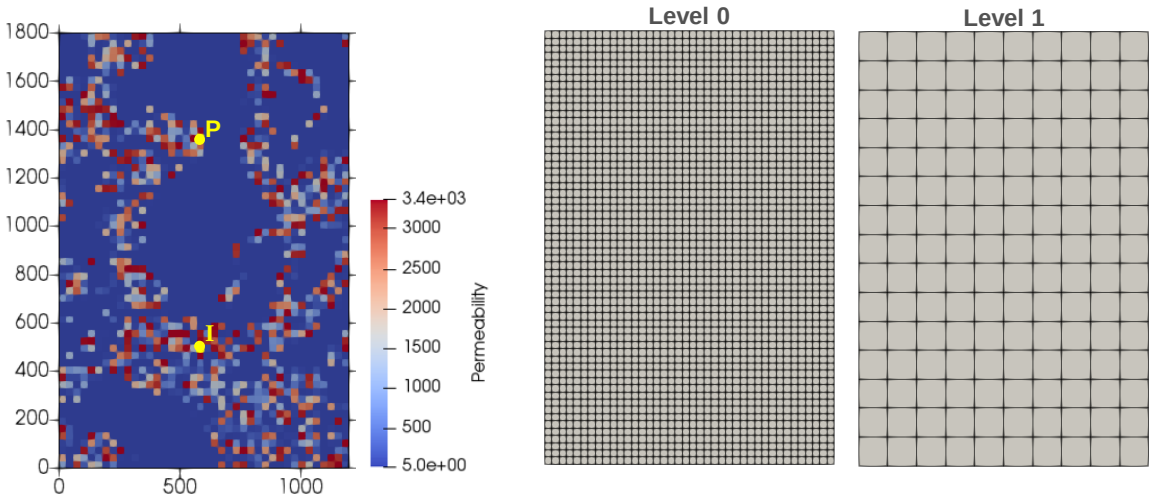

Figure 11 *Hierarchical grid of the heterogeneous model with low net-to-gross ratio. Left figure: permeability field with reservoir dimensions and well locations; middle figure: level 0, the finest level of refinement; right figure: coarser level, level 1.*

The simulation was conducted until cold water breakthrough reached the producing well. Figure 12 below illustrates the temperature solution at different times throughout the simulation. For each time shown, figure (a) represents the fine-scale solution, figure (b) is the AMR solution, and figure (c) is the coarse-scale solution. The grid is kept at its finest level at well locations.

The AMR mesh exhibits a significant improvement in temperature solution compared to the solution on the coarse grid. Refinement is mainly focused at the front and slightly beyond the front, while areas where insignificant changes occur remain coarse. Important details, such as fingering effects at the cold water front, which are neglected on the coarse grid, are clearly visible in both fine and AMR solutions, which results in a more accurate representation of this physical phenomenon.

The relative error throughout the simulation run was recorded, where the fine model is taken as reference

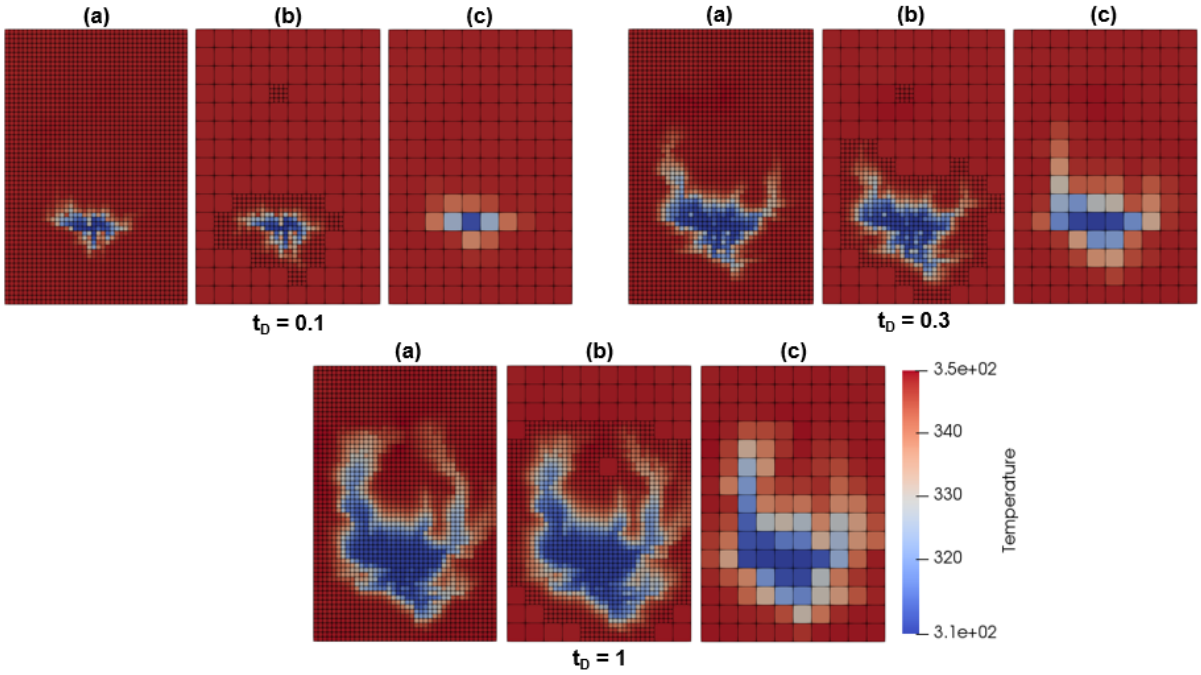

Figure 12 *Temperature solution of the heterogeneous model with low net-to-gross ratio at three different times: at t_D = 0.1, 0.3 and 1. (a) is the fine-scale solution (level 0); (b) is the AMR solution; (c) is the coarse-scale solution (level 1).*

solution, for comparison between the coarse and AMR model. Figure 13 below shows the L2 norm and the L-infinity norm error in time.

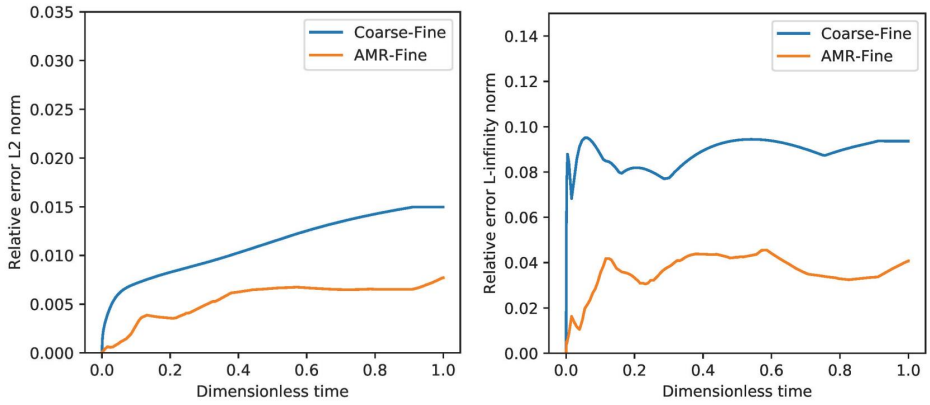

Figure 13 *L2 norm (left) and L-infinity norm (right) of the difference between the coarse model and the fine model, and between the AMR model and the fine model, both relative to the fine-scale solution, for the heterogeneous model with low net-to-gross ratio from figures 11 to 12.*

As can be seen, the marked improvement is also recorded in the error analysis, where the error between the coarse and fine model is notably larger than the error between the AMR and fine model. The L2 norm remains relatively constant for the AMR solution whereas it increases slightly in time for the coarse solution.

The amount of grid-cells used in the simulation ranges from 8 to 70% throughout the simulation (see figure 14). This represents a significant improvement in computational effort and time, while still capturing important features.

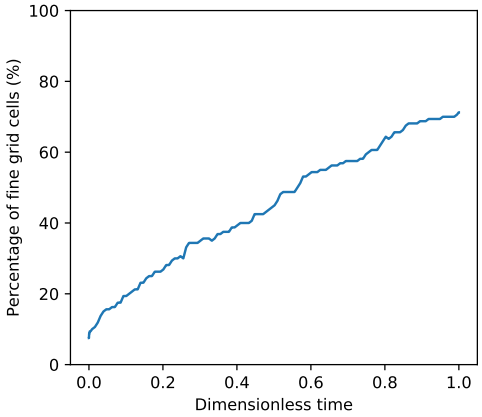

Figure 14 *Percentage of mesh elements used during the simulation of the AMR model, relative to the total number of cells in the fine-scale model in time for the heterogeneous model with low net-to-gross ratio from figures 11 to 12.*

Conclusions

This study aimed at developing an Adaptive Mesh Refinement (AMR) technique in *Delft Advanced Research Terra Simulator* for general-purpose reservoir simulation. The developed AMR framework consists of a multi-level hierarchical grid, where levels are constructed through a mesh partitioning of the fine-scale model - the static geological model - which is represented by a list of properties (e.g. volume and porosity). The framework consists of the construction of the coarse levels through cell aggregation of the next consecutive fine level at the pre-processing stage. The method used to aggregate fine cells includes the grouping of subdomains whose centroids are found within a predefined 3D domain. In this study, domains are grouped by the partitioning of the x-, y- and z- axes into equidistant intervals.

The aggregation of the subdomains to form a coarser level is stored as a list of indices for next stages, which consists of the indices of the fine cells comprised in its coarse control volume for each coarse cell. Next, in order to solve the relevant governing equations, the flow must be computed at each interface present in the mesh. We therefore generate a list - called a connectivity list - describing all neighbouring cells within each level and between levels. The fine-scale transmissibility is then computed using the permeability field. Hereafter, a flow-based upscaling is applied in order to acquire the transmissibility of coarser levels, and the inter-level transmissibility. Each control volume has defined parameters which are relevant for solving the system (volume, porosity, depth etc).

Once the hierarchy of levels is complete, the simulation can be started. Adaptivity check is performed at every time step, using criteria specific to the application. Once the regions for coarsening and refinement are defined, the solution is prolongated to the finest meshing level, and subsequently restricted from fine to the adaptive simulation grid. A new connection list and grid properties are constructed for the new coarsened schema. Once it is completed, the simulation runs for the next time step using the constructed simulation model.

The accuracy of the method was demonstrated for geothermal applications. Two models were tested, including a homogeneous model with unstructured gridding and a heterogeneous fluvial system model with low net-to-gross ratio. High levels of solution accuracy relative to the reference fine-scale results are observed for both cases. An error analysis was conducted to record the differences between the AMR and the coarse solution relative to the reference fine-scale solution. The error resulting from the AMR model is significantly lower than for the coarse model, for all tested problems. The overall percentage of grid cells used in the AMR model relative to the fine-scale model is considerably decreased for most problems.

To conclude, the developed AMR method shows high levels of accuracy for both homogeneous and

heterogeneous models, and can be used for geothermal applications as well as for other applications implemented in DARTS. The number of cells in the AMR simulation, relative to the total number of cells of the finest level, is considerably reduced, which is very favourable in terms of efficient use of computational resources. The framework is applicable to two- and three-dimensional models and for unstructured as well as structured meshes. The applicability of the method to unstructured grids provides an effective means for solving complex geological systems.

Acknowledgements

We would like to thank the DARTS group for their assistance and help. We would also like to acknowledge financial support from the SFB1313 research group at University of Stuttgart and particularly like to thank Beatrix Becker and Prof. Rainer Helmig for their valuable time and help.

References

Bahrainian, S. S., & Dezfuli, A. D. (2014). A geometry-based adaptive unstructured grid generation algorithm for complex geological media. *Computers & geosciences*, *68*, 31–37.

Branets, L. V., Ghai, S. S., Lyons, S. L., & Wu, X.-H. (2009). Challenges and technologies in reservoir modeling. *Communications in Computational Physics*, *6*(1), 1.

Christensen, J., Darche, G., Dechelette, B., Ma, H., Sammon, P., et al. (2004). Applications of dynamic gridding to thermal simulations. In *SPE international thermal operations and heavy oil symposium and western regional meeting*.

Christie, M. A. (1996). Upscaling for reservoir simulation. *Journal of petroleum technology*, *48*(11), 1–004.

Cusini, M., van Kruijsdijk, C., & Hajibeygi, H. (2016). Algebraic dynamic multilevel (ADM) method for fully implicit simulations of multiphase flow in porous media. *Journal of Computational Physics*, *314*, 60–79.

Durlofsky, L. J. (2005). Upscaling and gridding of fine scale geological models for flow simulation. In *8th International Forum on Reservoir Simulation Iles Borromees, Stresa, Italy* (Vol. 2024, pp. 1–59).

Gong, B., Karimi-Fard, M., & Durlofsky, L. J. (2008). Upscaling discrete fracture characterizations to dual-porosity, dual-permeability models for efficient simulation of flow with strong gravitational effects. *SPE Journal*, *13*(01), 58–67.

Jenny, P., Lee, S., & Tchelepi, H. A. (2003). Multi-scale finite-volume method for elliptic problems in subsurface flow simulation. *Journal of Computational Physics*, *187*(1), 47–67.

Karimi-Fard, M., & Durlofsky, L. J. (2012). Accurate resolution of near-well effects in upscaled models using flow-based unstructured local grid refinement. *SPE Journal*, *17*(04), 1–084.

Karimi-Fard, M., & Durlofsky, L. J. (2014). Unstructured adaptive mesh refinement for flow in heterogeneous porous media. In *ECMOR XIV-14th European conference on the mathematics of oil recovery*.

Karimi-Fard, M., Gong, B., & Durlofsky, L. J. (2006). Generation of coarse-scale continuum flow models from detailed fracture characterizations. *Water resources research*, *42*(10).

Khait, M., & Voskov, D. (2018a). Adaptive parameterization for solving of thermal/compositional nonlinear flow and transport with buoyancy. *SPE Journal*, *23*, 522-534. doi: 10.2118/182685-PA

Khait, M., & Voskov, D. (2018b). Operator-based linearization for efficient modeling of geothermal processes. *Geothermics*, *74*, 7-18. doi: 10.1016/j.geothermics.2018.01.012

Khait, M., & Voskov, D. V. (2017). Operator-based linearization for general purpose reservoir simulation. *Journal of Petroleum Science and Engineering*, *157*, 990–998.

Lim, K.-T., Schiozer, D., & Aziz, K. (1995). A new approach for residual and jacobian arrays construction in reservoir simulators. *SPE Computer Applications*, *7*(04), 93–96.

Pau, G. S. H., Bell, J. B., Almgren, A. S., Fagnan, K. M., & Lijewski, M. J. (2012). An adaptive mesh refinement algorithm for compressible two-phase flow in porous media. *Computational Geosciences*, *16*(3), 577–592.

Sammon, P. H., et al. (2003). Dynamic grid refinement and amalgamation for compositional simulation.

In *SPE reservoir simulation symposium.*

Shetty, S., Voskov, D. V., & Bruhn, D. (2017). *Numerical strategy for uncertainty quantification in low enthalpy geothermal projects* (Unpublished doctoral dissertation). M. Sc. thesis. Department of Applied Earth Science. Delft University of Technology.

Trangenstein, J. A. (2002). Multi-scale iterative techniques and adaptive mesh refinement for flow in porous media. *Advances in Water Resources*, *25*(8-12), 1175–1213.

Van Batenburg, D. W., De Zwart, A., Boerrigter, P. M., Bosch, M., & Vink, J. C. (2011). Application of dynamic gridding techniques to IOR/EOR processes. In *IOR 2011-16th European Symposium on Improved Oil Recovery.*

Voskov, D. V. (2017). Operator-based linearization approach for modeling of multiphase multi-component flow in porous media. *Journal of Computational Physics*, *337*, 275–288.

Wang, Y., Hajibeygi, H., & Tchelepi, H. A. (2014). Algebraic multiscale solver for flow in heterogeneous porous media. *Journal of Computational Physics*, *259*, 284–303.

Willems, C. (2017). *Doublet deployment strategies for geothermal hot sedimentary aquifer exploitation: application to the Lower Cretaceous Nieuwerkerk Formation in the West Netherlands Basin* (Unpublished doctoral dissertation). Delft University of Technology.